NASA

Technical Memorandum 79655

The REPSAT Approach to Low-Cost GPS Terminals

J. W. Sennott, A. K. Choudhury, and R. E. Taylor

APRIL 1979

National Aeronautics and Space Administration

Goddard Space Flight Center
Greenbelt, Maryland 20771

TM 79655

THE REFSAT APPROACH TO LOW-COST GAS TERMINALS

J. W. Sennott, Howard University
A. K. Choudhury, Howard University
R. E. Taylor, NASA/GSFC

April 1979

GODDARD SPACE FLIGHT CENTER
Greenbelt, Maryland

THE REFSAT APPROACH TO LOW-COST GPS TERMINALS

J. W. Sennott, Howard University
A. K. Choudhury, Howard University
R. E. Taylor, NASA/GSFC

ABSTRACT

This paper describes a concept utilizing a geostationary reference satellite (REFSAT) that broadcasts navigation - aiding signals to low-cost civil-user terminals which employ the constellation of 24 NAVSTAR Global Positioning System (GPS) satellites for position determination.

The low-cost receiver design approach eliminates requirements for delay-lock tracking and Costas loops; relaxes local oscillator long-term stability requirements from ±0.01 parts per million (ppm) to ±10 ppm; and reduces required digital processor capability substantially - all of which lower production costs compared to military counterparts. A design goal is to achieve a civil-terminal receiver cost of $1000/set, or less, in volume production.

This paper describes the signal acquisition, tracking and position-fixing properties of such a low-cost, dual-channel, L-band, civil user receiver designed to receive both GPS navigation and REFSAT navigation-aiding signals.

CONTENTS

LIST OF FIGURES

LIST OF FIGURES (Continued)

LIST OF TABLES

THE REFSAT APPROACH TO LOW-COST GPS TERMINALS

I. INTRODUCTION

Present plans call for world-wide deployment, by mid-1985, of a constellation of 24 NAVSTAR Global Positioning System (GPS) satellites. Many excellent articles[1-3] are available detailing the satellite constellation, as well as the various classes of user equipments under development. Although the impetus for GPS has come primarily from the Department of Defense, the significance of a high-accuracy position and velocity determination capability, in three dimensions, has not gone unnoticed by the civil sector, specifically the Department of Transportation and the National Aeronautics and Space Administration (NASA). Various efforts are underway to ascertain the potential of GPS for aeronautical, space and surface navigation functions. A theme common to these efforts is the development of "low-cost" user equipment concepts which would enable early and wide-spread civil utilization.

In a recent article by T. A. Stansell,[4] one finds a good summary of the issues involved in realization of low-cost civil GPS equipment. As pointed out, one possible avenue to cost reduction is alteration of the present GPS signal structure, as realized by a modification to GPS spacecraft.

This paper describes the geostationary reference satellite (REFSAT) approach having the following distinct advantages:

1. No impact on DOD spacecraft or user equipment, while making full use of existing GPS C/A "coarse acquisition" signals.
2. Low civil-user terminal cost with potential for under $1000/set given large production quantities and Large Scale Integration (LSI) technology.
3. Provision of access/denial command system for civil community.

The REFSAT approach employs narrow-band carrier-acquisition and frequency-shift-keyed (FSK) data signals sent from a geostationary space platform, in a configuration depicted in Figure

1. An L-Band down-link transmission is sent at the lower edge of the GPS L1 (1575.42MHz) channel, and is passed by a common receiver front-end into dual-channel IF amplifiers.

Development of the REFSAT concept involved a careful examination of the signal processing functions performed by the conventional NAVSTAR GPS user terminal. A contrast between the REFSAT and conventional receiver functions are described in the simplified block diagram, Figure 2.

II. OVERVIEW OF THE GPS-REFSAT TERMINAL CONCEPT

Before examining the REFSAT user terminal hardware and software requirements it is worth while reviewing the GPS signal structure available to civil users, together with the requisite functions performed in the conventional terminal.

The operational GPS constellation will consist of 24 satellites in circular 10,900nmi orbits, in three 63° (or 55°) inclined planes of 8 each.[1] At least 6 satellites are in view at any one time, from any point on earth; on the average nine satellites are in view. Each contains an atomic time standard which, among other things, generates a periodic 1023 PRN reference C/A code with period of 10^{-3} seconds. A spread-spectrum, L-band, ranging signal is derived by employing bi-phase modulation. All satellite clocks are kept synchronized by ground station tracking. Each satellite has its own unique PRN sequence, and in this way the two-MHz-wide C/A channel works in a code-division multiple access mode. For military users, this has the important advantage of simultaneous ranging on two or more signals while offering anti-jamming protection.

In Table 1, below, we have summarized the various operations to be performed in deriving a position fix. These are grouped by major function: (1) signal acquisition, (2) signal tracking and (3) position fixing. In implementing each, several sub-functions are performed. We will now contrast the GPS and GPS-REFSAT terminal sub-functions.

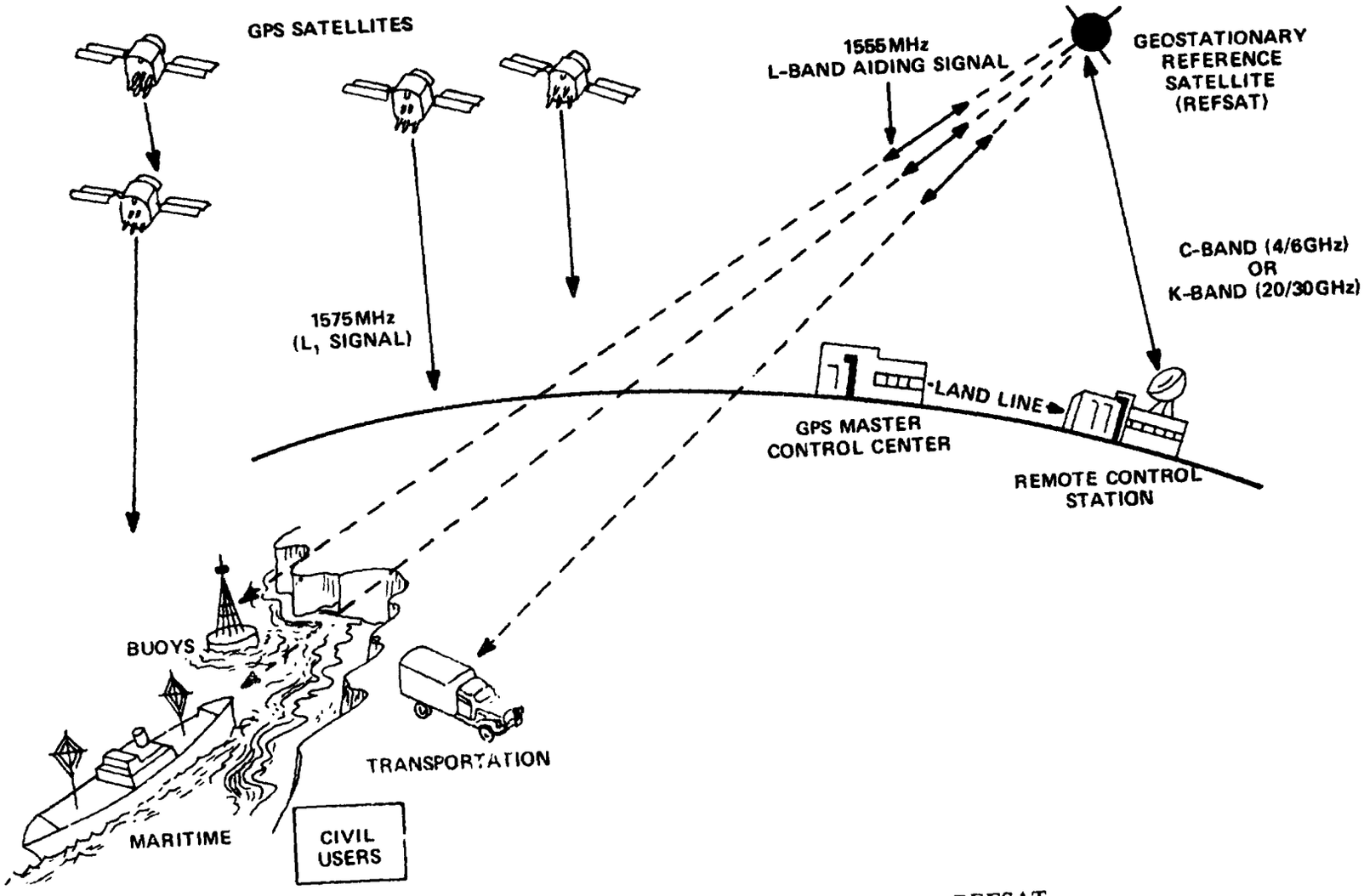

Figure 1. NAVSTAR GPS Concept Using Geostationary REFSAT

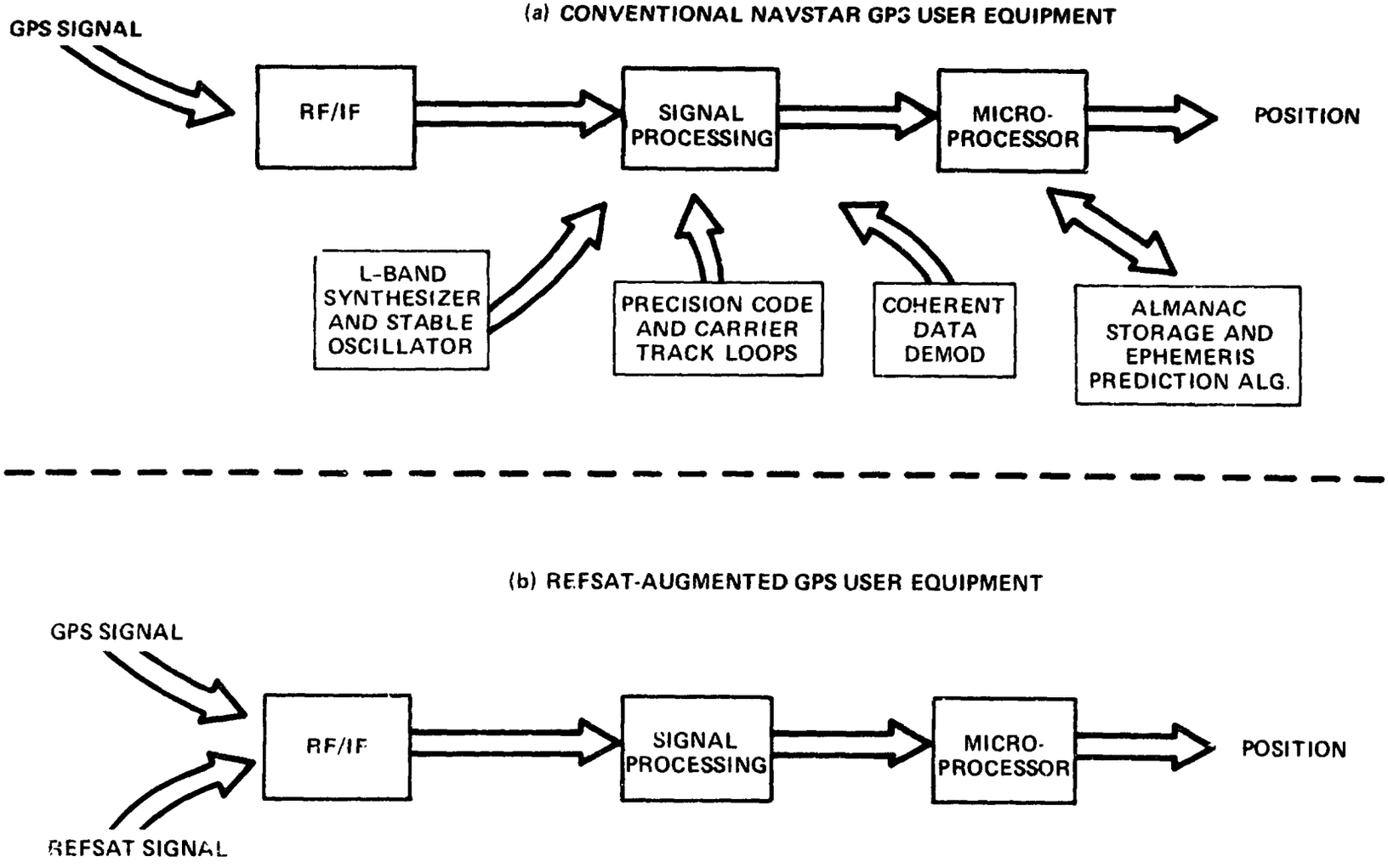

Figure 2. REFSAT vs. Conventional Receiver

Table 1
GPS Receiver Functions Comparison

		Conventional GPS Terminal		
Major Function	Sub-Function	Hardware	Software	REFSAT Simplification
Signal Acquisition	1. Initial Satellite Selection		GPS Almanac Compute satellites in view	Eliminate this software/ storage function
	2. Doppler Acquisition	1 part 10^7 synthesizer (in oven)	Compute range rate for selected satellites	VCXO to 1 part in 10^5
	3. Delay Acquisition	PSK spread spectrum programable synthesizer (in phase & quadrature)	Filter error signals Advance/retard commands	Reduce code generator precision
Signal Tracking	4. Fine Delay Track	Delay-lock loop	Filter error signals Advance/retard commands	No punctual code, employ interpolation
	5. Fine Doppler Acquisition	AFC loop	Filter error signals VCXO freq. step commands	Not essential for all users
	6. Carrier Phase Track	Costas loop	Filter error signals VCXO phase step commands	Eliminate entirely
Position Fixing	7. Telemetry Acquisition	PSK demodulate using above phase reference		Simple non-coherent FSK
	8. Ephemeris Update		Real-time predictor	Eliminate entirely
	9 Position Computation		Pseudo range to lat.-long. conversion	

In the conventional GPS terminal, signal acquisition begins with onboard computation of GPS satellites in view. To accomplish this, the terminal must know, approximately, its own location and have available a recent version of the GPS almanac. For acquisition to go forward, Doppler estimates must then be computed for the subset of GPS satellites having good geometry. This leaves the GPS demodulator, typically, with a-priori GPS carrier frequency uncertainty of several hundred hertz (Hz). However, to stabilize the receiver front-end local oscillator to this accuracy requires an oven-stabilized L-band synthesizer. To complete the signal acquisition function, the GPS receiver generates a local C/A code reference for each selected GPS satellite, and searches for the cross-correlation peak in 0.5-1.0 microsecond steps, spanning the 10^{-3} second code period.

The acquisition function, as performed in the GPS-REFSAT user terminal, differs from the above in several important aspects. Before examining these differences, the REFSAT down-link signal format, Figure 3, must be understood. The REFSAT signal structure consists of an FSK data stream divided into 128 bit sub-frames. Each contains a Doppler gradient word, C/A code select word and satellite position (referenced to REFSAT system frame epoch). The overall FSK transmission is centered on frequency ω_{RS}. Considering the GPS-REFSAT terminal acquisition function, the aided terminal first acquires the FSK data stream, which is accomplished with a non-coherent FSK demodulator. Since the REFSAT concept employs a dual-channel L-band receiver with a common L.O., drift effects are common to both the GPS and aiding signal. Thus, a long-term stability as poor as ±10ppm may be employed with no effect on Doppler acquisition. Also noteworthy is the satellite selection procedure which, in the GPS-REFSAT terminal, is developed directly from the FSK data words. The GPS-REFSAT terminal completes the signal acquisition function with a C/A code scan identical to that for the conventional terminal.

Consider now the signal tracking functions listed in Table 1. In the conventional GPS terminal signal tracking occurs in three stages. Firstly, the code delay must be tracked and an

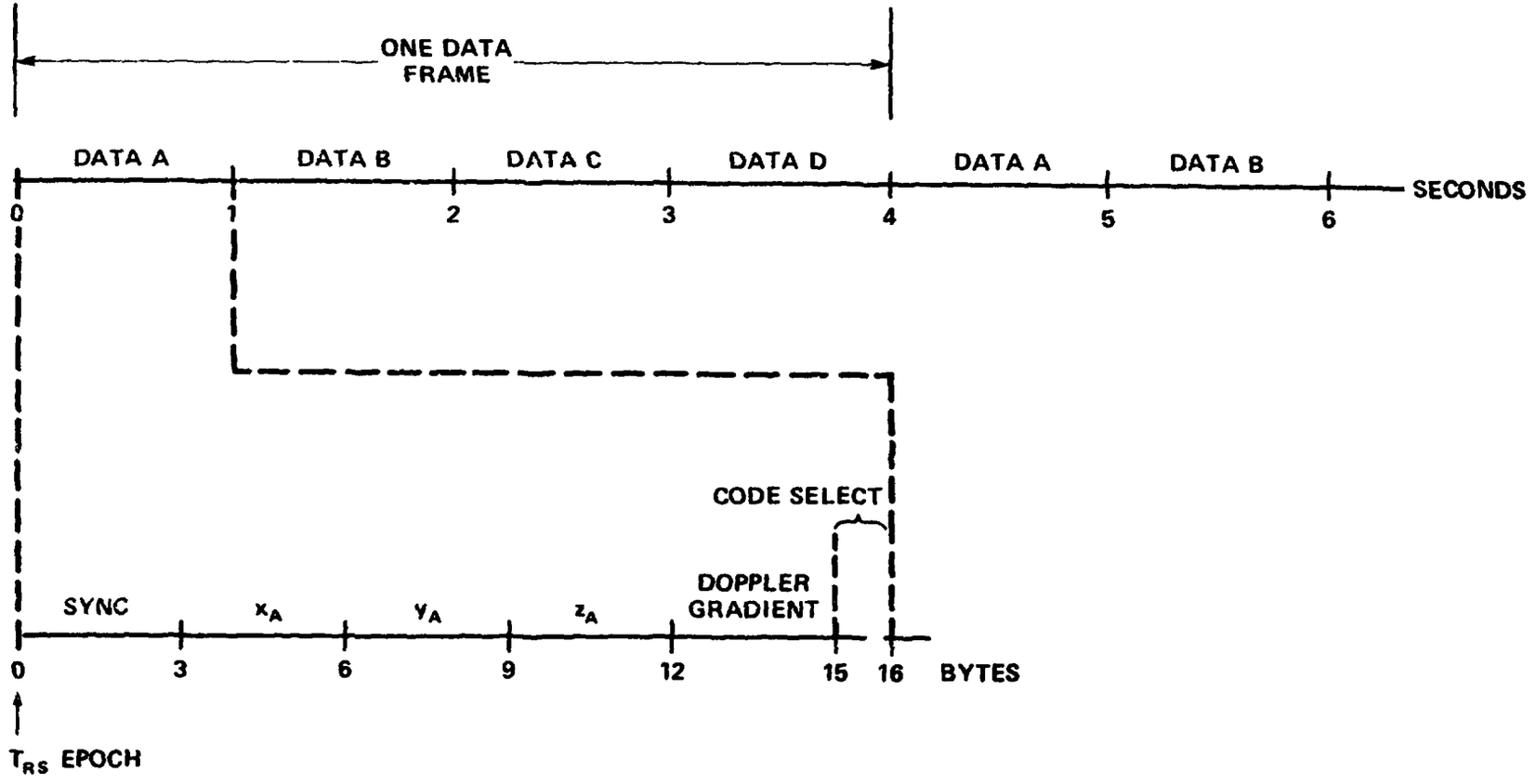

Figure 3. REFSAT Data Format

aligned or "punctual" code stream generated. This is implemented with either a delay-lock loop or tau-dither technique. Regardless, the end result must be a continuously tracked code generator with delay error held to within one-tenth of a microsecond or better. Secondly, Doppler uncertainty must be eliminated. This may be accomplished by stepping the frequency synthesizer and measuring correlator output. Once the Doppler uncertainty is reduced to 10-20Hz, carrier-phase and GPS data is recovered using a Costas loop and the aforementioned punctual code.

The GPS-REFSAT terminal performs the signal tracking function in a substantially different fashion. A continuously-tracked punctual code is not necessary. For most users a code-delay interpolation scheme is sufficient. With this technique, described in Section III, code step pairs separated by one chip are employed. This simplifies the code generators and tracking filters. Further, the Costas carrier phase tracking loop is eliminated.

The user terminal function performed last is position fixing. As shown in Table 1, this is composed of three sub-functions. In the conventional terminal ephemeris parameters, contained within the 50 B/S data message, are updated hourly. The GPS terminal employs these parameters, together with a software model for the satellite orbits, to compute satellite coordinates in real time. This requires substantial memory and computational resources. Given time delay (and Doppler) estimates, the GPS receiver then computes position, time, velocity and bias variables of interest.

The GPS-REFSAT terminal, on the other hand, offers a simplification. The REFSAT FSK data stream (Figure 3) provides, every four seconds, updated GPS satellite coordinates. This eliminates most of the storage and computation associated with hourly updating of GPS satellite ephemeris parameters. In Section V, we will discuss the position fix and satellite co-ordinate update approach in more detail

At this point, it is useful to present simplified block diagrams for the conventional and aided-user terminals, Figures 4 and 5 respectively For the conventional terminal we have assumed a

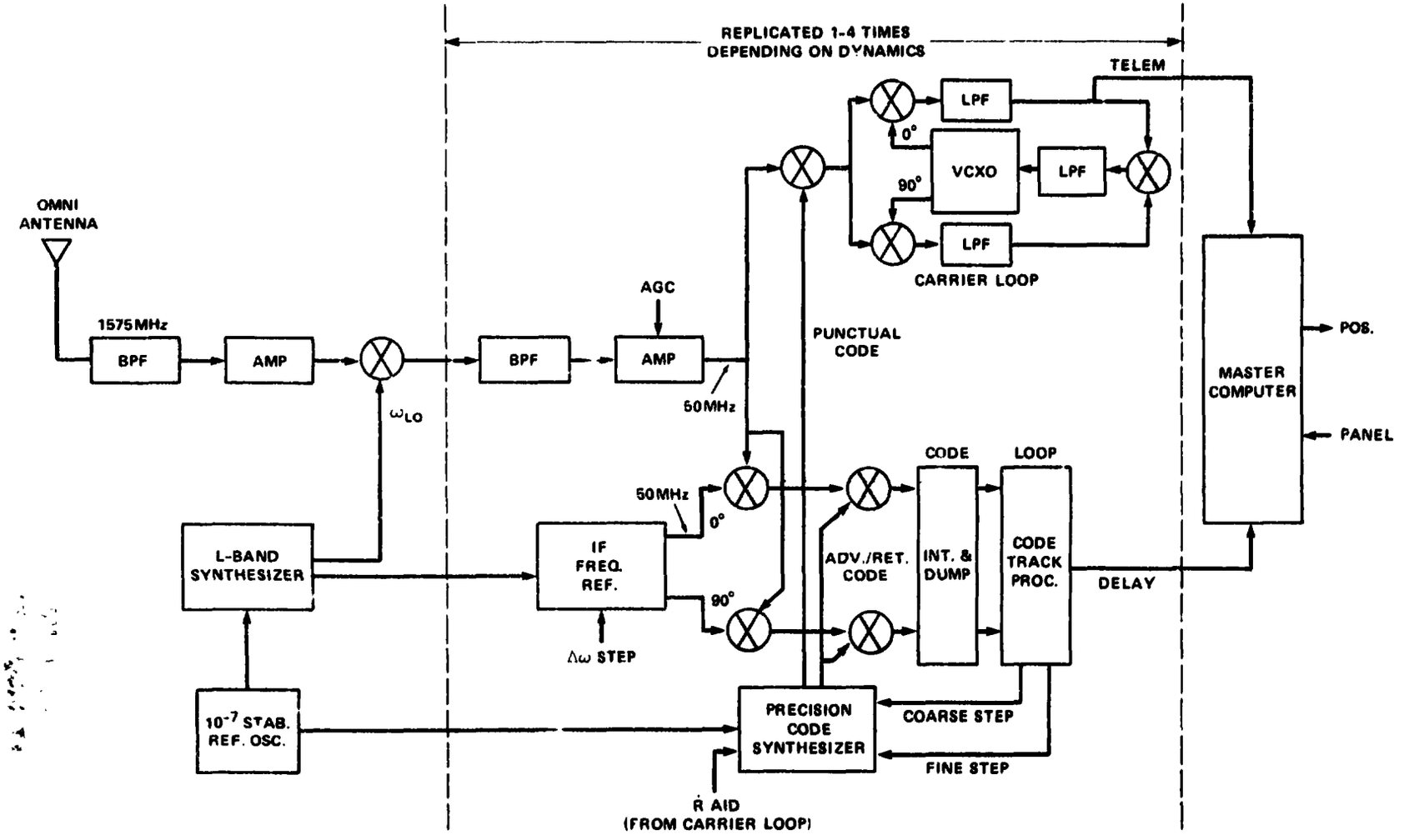

Figure 4. Simplified Block Diagram Un-aided GPS Terminal

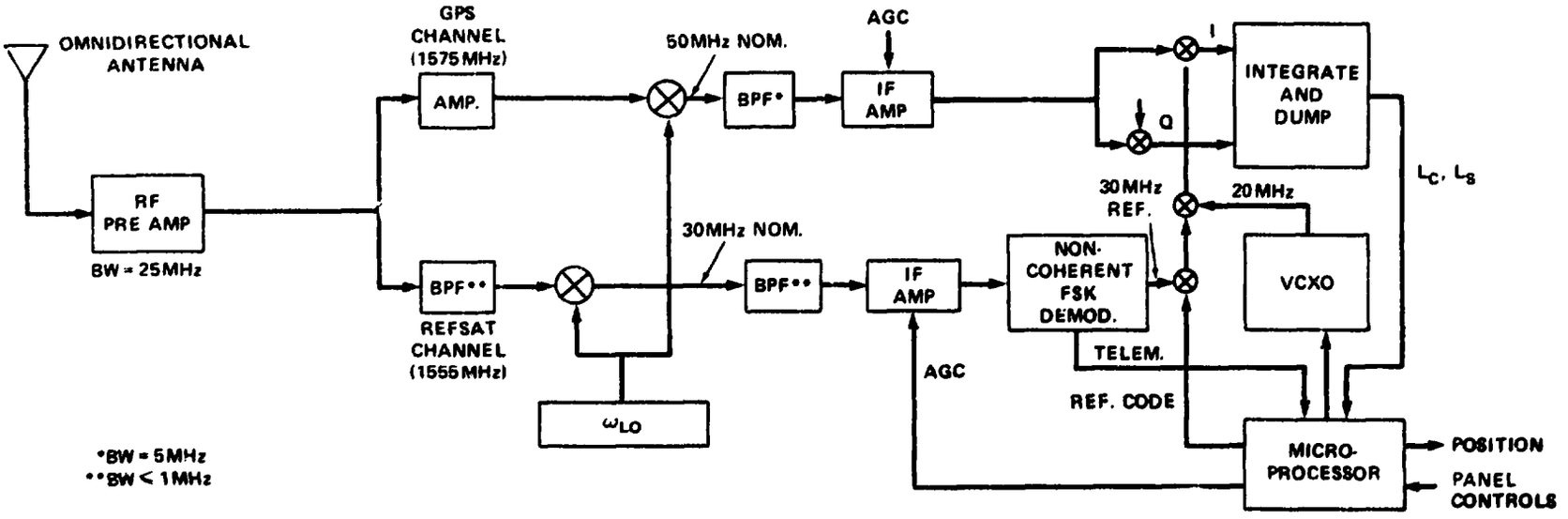

Figure 5. Simplified Block Diagram REFSAT User Terminal

"single-channel" version in which acquisition and tracking circuitry is shared, sequentially, between different GPS satellites. Components in the GPS receiver include RF/IF hardware, L-band synthesizer and frequency reference, code tracking loop, carrier tracking loop and digital processor. For the GPS-REFSAT receiver the L-band synthesizer and reference have been eliminated, along with punctual code and Costas loop components. Further, the code generator and digital processor have been simplified.

In the following sections a more detailed description (and analysis) of the acquisition, tracking and position fixing functions is provided.

III. SIGNAL ACQUISITION

At the user terminal a given GPS satellite signal will be buried in both additive Gaussian noise and signals from six to eight other GPS satellites. The desired signal is received with unknown Doppler and range delay. Ultimately, the receiver must compute the relative Doppler and delay between this satellite and all others which may be visible. The initial acquisition function is carried out with an M-ary hypothesis test, over the appropriate range time-delay and Doppler frequency cells. In mechanizing the above test it becomes necessary to generate, locally, time and frequency-shifted C/A codes. One then generates the in-phase and quadrature correlations, I and Q. Under microprocessor control, a family of statistics are generated by sweeping out the total Doppler and delay uncertainty. These non-coherent statistics are denoted by $\Lambda(i,j)$, where i and j are code and VCXO indexes, respectively.

Under noiseless conditions, a given $\Lambda(i,j)$ appears in Figure 6. A maximum correlation value results when the received delay and Doppler parameters match those generated by the local code and voltage controlled crystal oscillator (VCXO). Correlation on the time delay axis is essentially zero beyond 10^{-6} seconds offset, with the Doppler zero-crossing at 10^{3} Hz. With channel noise present a delay-Doppler pair (i,j) far removed from the peak may yield maximum correlation. The probability of such an event, computed in the Appendix, is denoted as $P_H[E]$. To combat this type of error, a sequential test is employed.

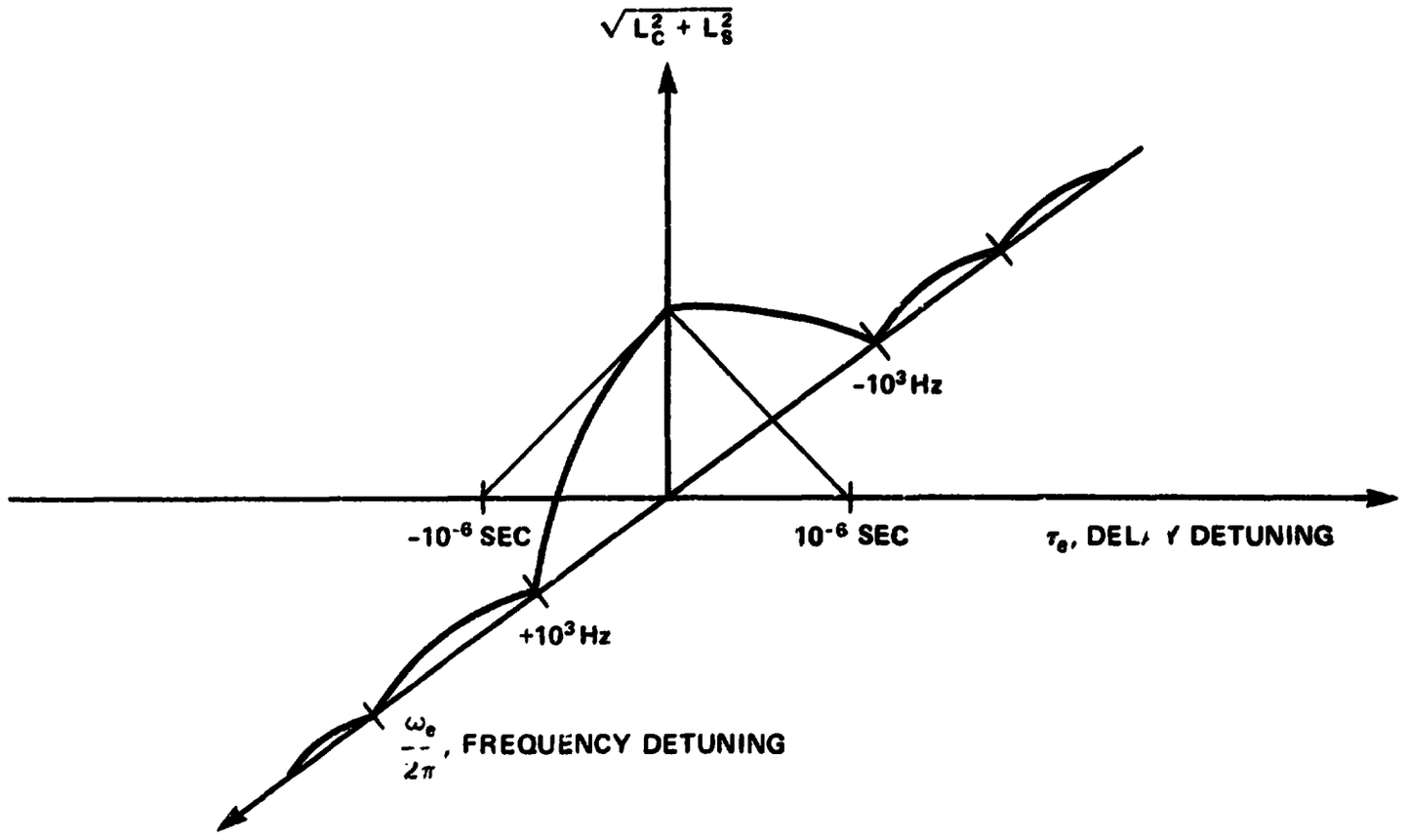

Figure 6. Correlator Response vs. Detuning (10^{-3} sec integration)

This approach uses a "run comparison" threshold. Statistic $\Lambda(i,j)$ is compared with $\Lambda(i-1,j)$, m times. If $\Lambda(i,j) > \Lambda(i-1,j)$ in each test, a "hit" is registered. The process is repeated until the total set of delay indexes is searched, or a "hit" is registered. If the number of delay steps to be scanned is s, then the probabilities of interest are computed to be:

$$P_r \text{ [start false track]} = s\,(1/2)^m \tag{1}$$

$$P_r \text{ [detect true delay]} = [1 - P_H(E)]^m \tag{2}$$

$$P_r \text{ [dismiss true delay]} = 1 - [1 - P_H(E)]^m \tag{3}$$

Doppler uncertainty, affecting values of $P_H(E)$, expressed by the Marcum-Q function defined in the Appendix is a predominant factor. Figure 6 shows the rapid fall-off of correlation with increasing frequency offset. The entire delay index scan is repeated for each 200Hz - increment of Doppler uncertainty.

The observed Doppler will be different at each receiver. For the CONUS, total Doppler span for each satellite is approximately 4kHz. Typical Doppler contours are shown in Figure 7; the gradient is about one Hz/km. Now if the receiver has some a-priori knowledge of position, say to ±150km, an initial prediction of Doppler to several hundred Hz can be made. However, a single-channel receiver's L-band stability must be this accurate as well since a prolonged Doppler scan would be necessary. As discussed previously, the REFSAT dual-channel receiver solves this problem. Also, the REFSAT carrier can be transmitted with a known frequency offset relative to the GPS satellites of interest. The received frequency offset may then be computed by the user, by making use of the Doppler gradient word and an initial position estimate. The frequency detuning error (radian per second) as seen at the receiver is:

$$\omega_e = \left\{ |\dot{\underline{r}}_O - \dot{\underline{r}}_A| \frac{\omega_{GPS}}{C} - \omega_{LO} \right\} - \left\{ |\dot{\underline{r}}_O - \dot{\underline{r}}_{RS}| \frac{\omega_{RS}}{C} - \omega_{LO} + j\Delta\omega \right\} \tag{4}$$

Eq. (4) reflects the RF/IF structure of Figure 5. As previously noted, the ω_{LO} term cancels because of the dual-channel receiver. Additionally, for many users, the user-to-REFSAT range-rate

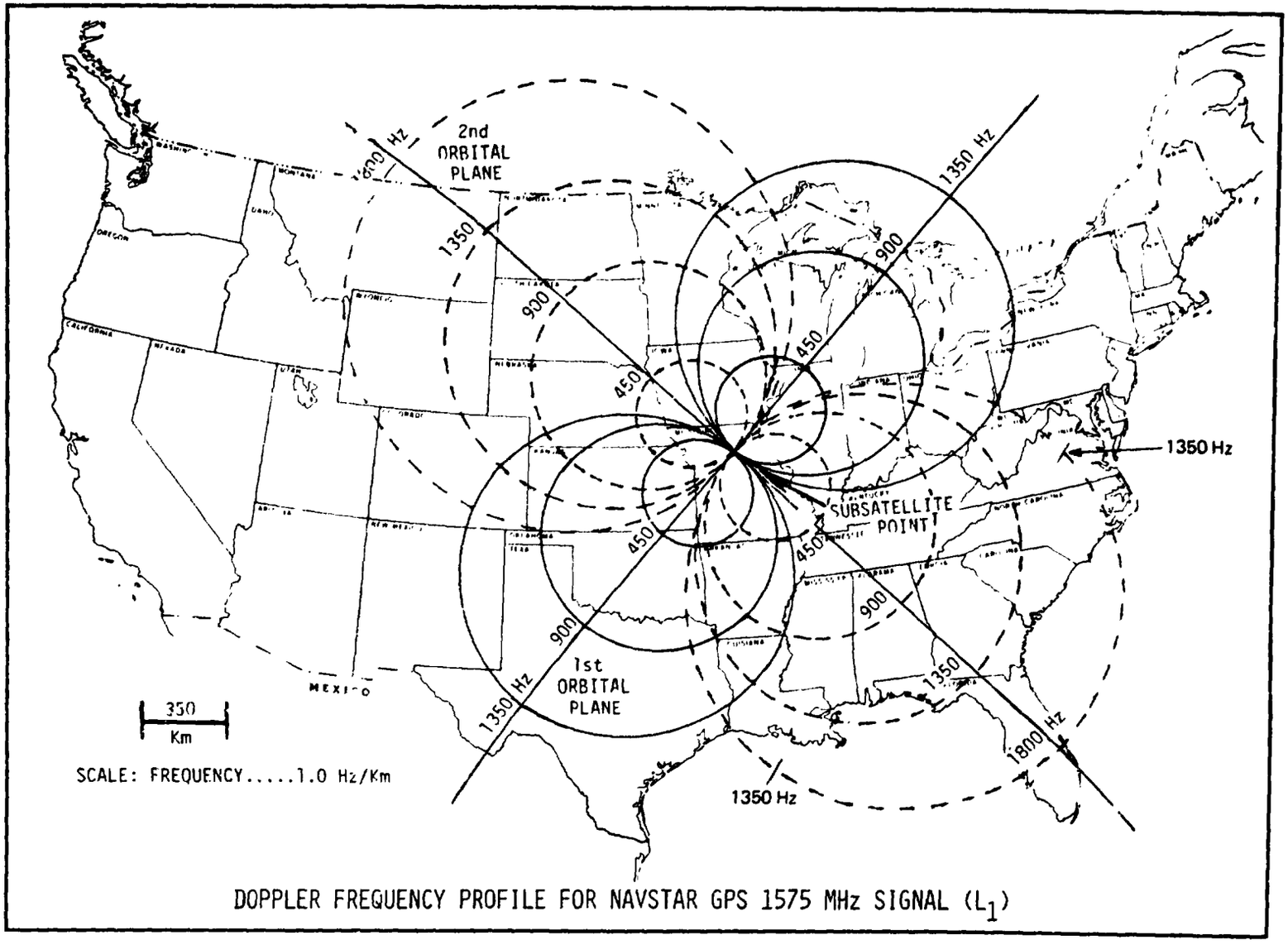

Figure 7. Typical Doppler Contours

term, $|\dot{r}_o - \dot{r}_{RS}|$, is small. The initial value of j is then found from;

$$j\Delta\omega = |\dot{\underline{r}}_o - \dot{\underline{r}}_A| \frac{\omega_{GPS}}{C} \tag{5}$$

where the term on the right of Eq. (5) may be estimated from the REFSAT Doppler gradient word for GPS satellite A.

Returning now to Eqs. (1-3), let us assume that the Doppler detuning error has been reduced to within 150Hz. Considering delay-detuning, the worst-case condition is clearly for an arrival time which is exactly between two delay steps, and on the average the error is $0.25\Delta\tau$. Now going to the 43dB-Hz performance curves, Figure 11 of the Appendix, the false hypothesis probability $P_H(E)$ is 0.008. Using a run repeat index value m = 10 yields a "start false track" probability of 0.976 and a "detect true delay" probability of 0.93. This is for the worst-case in which all 1023 delays must be scanned before getting to the correct delay. In this situation one false track may be passed to the track verification phase but, with probability 0.93, the true track will be included as well. The overall scanning process, for m = 10, requires about 20 seconds per satellite. Total acquisition time for 4 GPS satellites would be on the order of 80 seconds.

A hybrid analytical/simulation model will be developed to obtain more exact performance statistics involving received signal strength and the parameters s and m.

IV. TRACKING AND INTERPOLATION

Unlike the acquisition mode, wherein many Λ values may have to be scanned, once tracking commences index gates are continually available for each of the satellites A, B, C, and D. These are maintained in a repeat-scan fashion whereby codes A, B, C, and D are checked sequentially using the two closest values of step index, say i and i + 1. In all, eight statistics are generated and checked during each cycle. The process is repeated every 12 milliseconds, depicted in Figure 8. An interpolation scheme is then employed to generate the time delays used in position

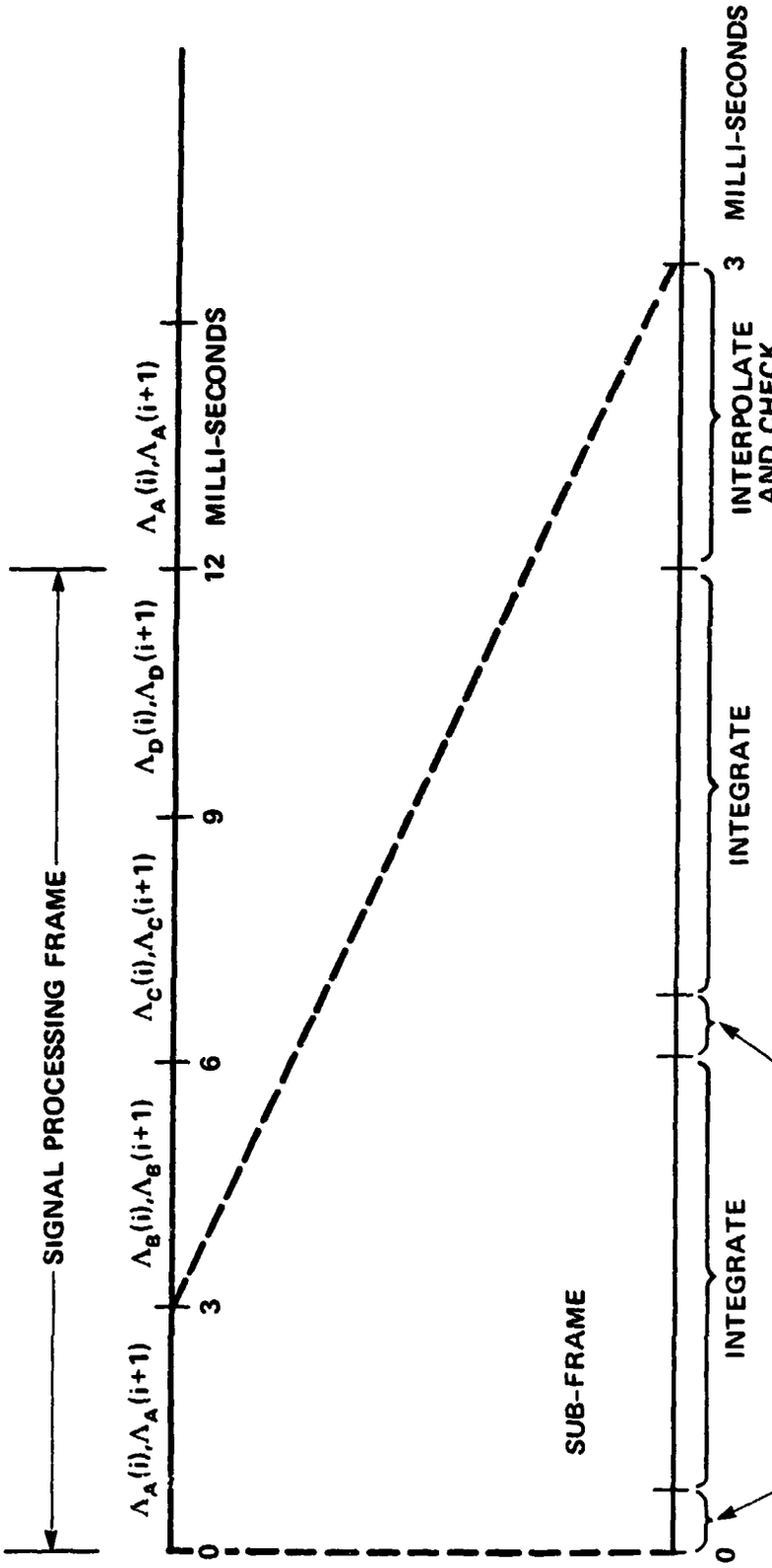

Figure 8. Signal Processing Sequence

computation. As pointed out in Section II, this can be done since a punctual code is not required. For satellite A, the time delay estimate is given by:

$$\hat{\tau}_A = i_A \Delta\tau + I_A \tag{6}$$

where, for

$$\Lambda_A(i,j) > \Lambda_A(i+1,j);$$

$$I_A \equiv \left\{1 - \frac{[\Lambda_A(i,j)]^{1/2} - [\Lambda_A(i+1,j)]^{1/2}}{[\Lambda_A(i,j)]^{1/2} + [\Lambda_A(i+1,j)]^{1/2}}\right\} \frac{\Delta\tau}{2} \tag{7}$$

The interpolation function I_A is composed of the difference of two adjacent test statistics, normalized by a gain constant formed from their sum. In Figure 9, we have plotted I_A and Λ, for noiseless conditions, as a function of code delay offset $\Delta\tau_e$. Interpolation standard deviation is developed in the Appendix and tabulated below for a range of carrier-to-noise (CNR) ratios:

CNR	$\Delta\tau = 10^{-6}$ sec.	$\Delta\tau = 0.5 \times 10^{-6}$ sec.
(40dB-Hz)	120m.	60m.
(43dB-Hz)	75m.	37m.
(46dB-Hz)	60m.	30m.

It is significant to point out that the above "raw" errors can be reduced substantially, for most civil-user applications, by post-interpolation smoothing. Furthermore, the observations can be updated rapidly, at a maximum rate of about 80 times/sec., making them suitable for certain high-dynamics user applications.

A typical signal processing sequence, controlled by the microprocessor, is depicted in Figure 8 for four, visible, GPS satellites. Implicit in this sequence are the following operations:

- Recent interpolations are averaged.
- Interpolations far removed from average are edited out.
- Code phase step is incremented or decremented when the average interpolation is outside specified limits.

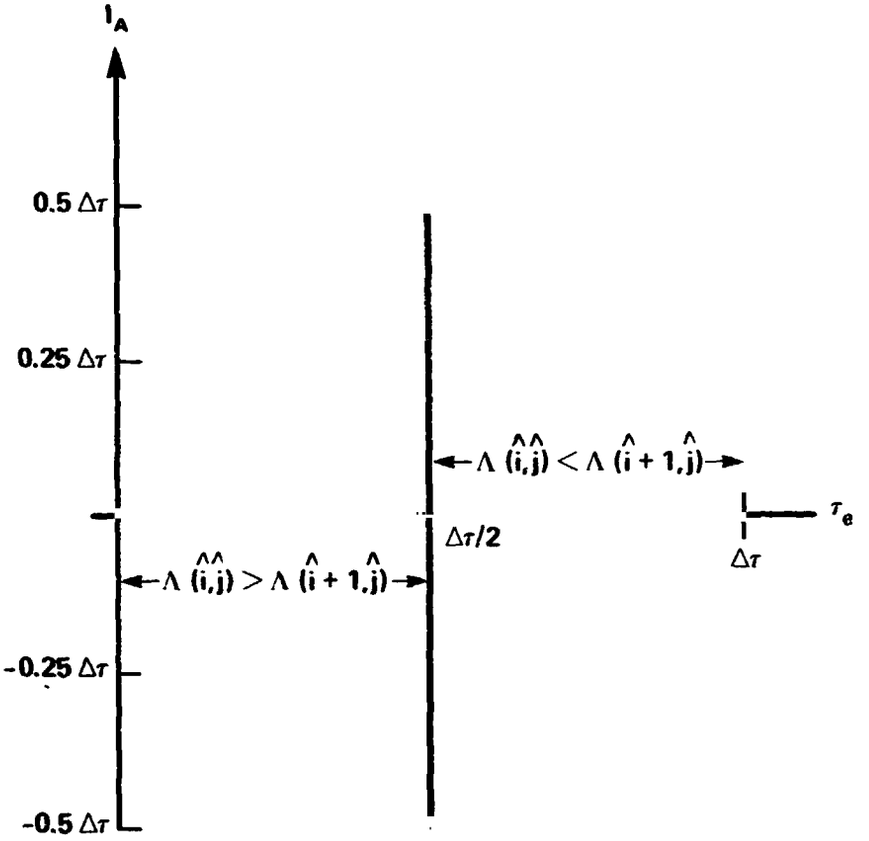

(a) CODE-DELAY INTERPOLATION FUNCTION

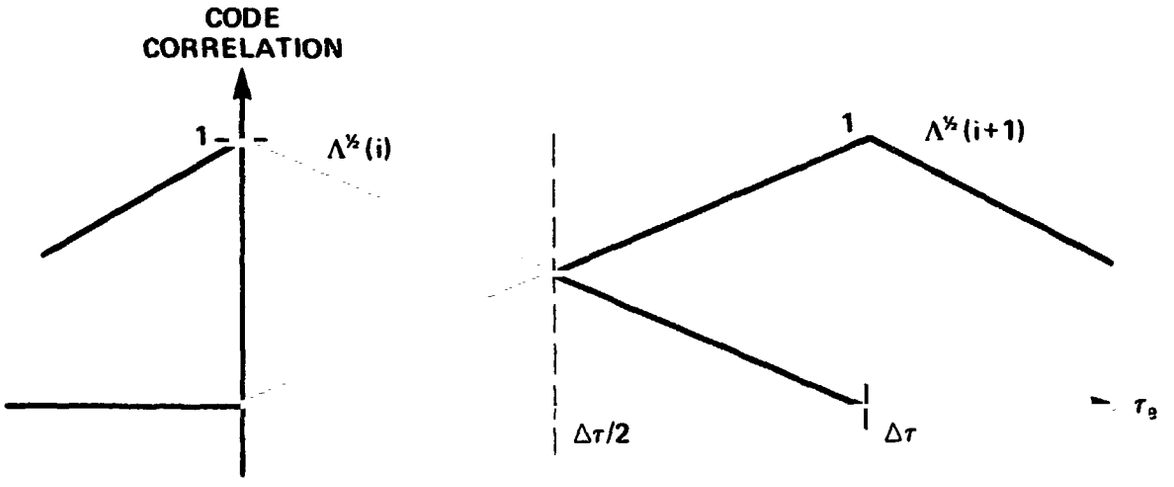

(b) CORRELATION-INTERPOLATION COMPONENTS

Figure 9. Code-Delay Interpolation Function and Correlation-Interpolation Components

V. POSITION FIXING

The REFSAT-aided receiver must, as does the conventional GPS receiver, convert estimated code arrival times into user position. In either case, the solution depends upon a knowledge of GPS satellite positions at the instant of ranging code transmission. The GPS-REFSAT receiver microprocessor keeps track of these positions by decoding the REFSAT FSK data stream (Figure 3), which contains direct coordinate information referenced to the GPS C/A code period emitted at event time T_{RS}. The REFSAT approach eliminates the need for satellite dynamical models, and associated computations, normally required. The method for obtaining a user position fix will now be discussed in more detail.

In visualizing the various event times, it is helpful to view each C/A code period of 1023 chips as a single pulse, emitted by the GPS satellite at the onset of that period. We neglect in this discussion the small clock offsets which exist between different GPS satellite clocks, and assume that all codes are synchronized. Every four seconds the REFSAT system defines one of these synchronous emission times as having occurred at T_{RS}. If but one set of pulses were emitted by the GPS satellites every four seconds, and if the receiver could measure the arrival times on parallel channels, the signal arrival times for GPS satellites A, B, C and D would be:

$$\tau_A = |\underline{r}_o(\tau_A) - \underline{r}_A(T_{RS})|/C + T_{RS} \tag{8}$$

$$\tau_B = |\underline{r}_o(\tau_B) - \underline{r}_B(T_{RS})|/C + T_{RS} \tag{9}$$

$$\tau_C = |\underline{r}_o(\tau_C) - \underline{r}_C(T_{RS})|/C + T_{RS} \tag{10}$$

$$\tau_D = |\underline{r}_o(\tau_D) - \underline{r}_D(T_{RS})|/C + T_{RS} \tag{11}$$

The observed delay estimates, $\hat{\tau}_i$, are equated to the above theoretical delay values to get:

$$\hat{\tau}_A = |\hat{\underline{r}}_o(\tau_A) - r_A(T_{RS})|/C + \hat{T}_{RS} \tag{12}$$

$$\hat{\tau}_B = |\hat{\underline{r}}_o(\tau_B) - r_B(T_{RS})|/C + \hat{T}_{RS} \tag{13}$$

$$\hat{\tau}_C = |\hat{\underline{r}}_o(\tau_C) - \underline{r}_C(T_{RS})|/C + \hat{T}_{RS} \tag{14}$$

$$\hat{\tau}_D = |\hat{\underline{r}}_o(\tau_D) - r_D(T_{RS})|/C + \hat{T}_{RS} \tag{15}$$

In solving these the (usual) assumption is made that $\underline{r}_o$, user position, is constant between pulse arrival times, and that the GPS satellite positions at the reference time are accurately known. The latter information is encoded directly with REFSAT data blocks A-D (Figure 3). Each coordinate is encoded with 23-bit accuracy, for an error of about 2 meters. In solving for $\underline{r}_o$, the microprocessor also provides T_{RS}. A time-of-day word encoded at the start of each data block may then be used to set the user clock with that of the ground stations.

The idealized scheme above is complicated by the fact that GPS code periods are emitted every millisecond, with receiver interpolation accomplished sequentially over a 12 millisecond interval. Further, the user may want position fixes anytime during each frame. In such cases, the receiver software must account for GPS satellite motion from positions at T_{RS}. This is a straightforward procedure, assuming the user position is known to within several hundred km. The "offset" satellite positions, at k_i code periods following T_{RS}, are estimated to be:

$$\hat{\underline{r}}_i\,(T_{RS} + k_i\Delta T) = \underline{r}_i\,(T_{RS}) + k_i\Delta T\hat{\underline{r}}_i \qquad (16)$$

Satellite velocity estimates $\hat{\underline{r}}_i$ of sufficient accuracy result simply by differencing satellite position between data frames. Worst-case satellite positioning error is on the order of 7 meters, plus any uncertainty due to ground control station tracking.

The major position-fixing error sources have been tabulated in Table 2, for three different position fix rates. For fixes smoothed over one second the delay estimation contribution is 6.7 meters, whereas for very high update rates this term contributes as much as 60 meters. For most civil users, the dominant error source will be due to ionosphere propagation. A 35-meter value is worst-case, and about an order of magnitude larger than experienced at most times. Nevertheless, it may be desirable to include a propagation correction word in each of the REFSAT data blocks. Analogous to the Doppler gradient word, this would allow a direct correction in real-time, given approximate knowledge of user position. Such a scheme should allow position fixing to substantially better than 100 meters.

Table 2
Error Budget Summary

Error Terms	fix rate[1] 1 per sec	fix rate[1] 10 per sec	fix rate 80 per sec
(2) delay estimation (40dB-Hz CNR)	6.7m	21m	60m
(3) GPS satellite positioning	9 m	9m	9m
(4) propagation uncertainty	35 m	35m	35m
(5) GDOP multiplier	3:1	3:1	3:1
Total fix error	152 m	195m	312m

Notes:

(1) assumes constant velocity and independent range-rate solution,
(2) interpolation performed with 1/2 chip offset,
(3) 2-m error contribution from GPS Master Control Center and 7-m from REFSAT FSK encoding,
(4) may be reduced with REFSAT propagation correction transmission,
(5) Geometric Dilution of Precision (GDOP).

VI. FUTURE ACTIVITIES

NASA is planning to demonstrate, operationally, the REFSAT concept during CY 1979; a "breadboard" REFSAT user-terminal receiver is currently being designed for this purpose. NAVSTAR GPS Phase I satellites (6 expected in orbit by Fall-1979) will be employed to determine geographical location with the breadboard REFSAT receiver.

The operational demonstration of the REFSAT concept will be backed up with a software simulation and analysis model for determination of user terminal position error.

By mid-1979, a detailed cost analysis of a REFSAT user terminal design will be completed to ascertain if low-cost production cost goals can be achieved.

VII. CONCLUSION

The REFSAT-aided GPS concept appears to offer significant advantages th ontribute to low user terminal production cost, as evidenced by reduced electronic circuit complexity, and relaxed-component precision.

The REFSAT approach eliminates delay-lock tracking and Costas loops, relaxes receiver front-end local oscillator long-term stability requirements; and reduces microprocessor requirements by eliminating satellite almanac and satellite positioning computations-all of which lower production costs compared to military counterparts. The GPS C/A code navigation performance capability has not been sacrifi..d, making the navigation capability, for example, more accurate than LORAN-C or VORTAC.

APPENDIX

TEST STATISTIC ANALYSIS

The REFSAT user terminal generates non-coherent code correlation test statistics making use of the signal processing approach discussed previously, Figure 8. Such statistics are employed both during signal acquisition and interpolation (tracking). The following analysis is similar to that for non-coherent radar and non-coherent orthogonal data systems.

Consider first an equivalent noise model for Figure 5, as Figure 10. All GPS channel noise, including that from the front-end L-band mixer and VCXO mixer, is replaced by a single noise source of N_G watts/Hz. The noise level is referenced to a unit-amplitude carrier. The Doppler and delay detuning errors between the two signal paths are $\omega_e = \omega - \omega'$ and $\tau_e = \tau - \tau'$, respectively. In-phase (I) and quadrature (Q) channel outputs following integration are:

$$I_C = \int_{t_i}^{t_i + \Delta T} \left\{\cos[\omega t + P(t - \tau) + \phi] + W_G(t)\right\} \left\{\cos[\omega' t + P(t - \tau') + \phi]\right\} dt \qquad (17)$$

$$L_S = \int_{t_i}^{t_i + \Delta T} \left\{\cos[\omega t + P(t - \tau) + \phi] + W_G(t)\right\} \left\{\sin[\omega' t + P(t - \tau') + \phi]\right\} dt \qquad (18)$$

In forming the sum-square statistic from these quantities, the phase error term $\phi - \phi'$ is eliminated.

We first observe that both L_C and L_S are Gaussian random variables. Working on their expectations, and replacing the 0, π function $P(\cdot)$ with a function $P'(\cdot)$ which takes on values ± 1, we have:

$$E[L_C | \omega_e, \tau_e] = \int_{t_i}^{t_i + \Delta T} P'(t - \tau)P'(t - \tau')\cos[\omega t + \phi]\cos[\omega' t + \phi']dt \qquad (19)$$

$$E[L_S | \omega_e, \tau_e] = \int_{t_i}^{t_i + \Delta T} P'(t - \tau)P'(t - \tau')\cos[\quad + \phi]\sin[\omega' t + \phi']dt \qquad (20)$$

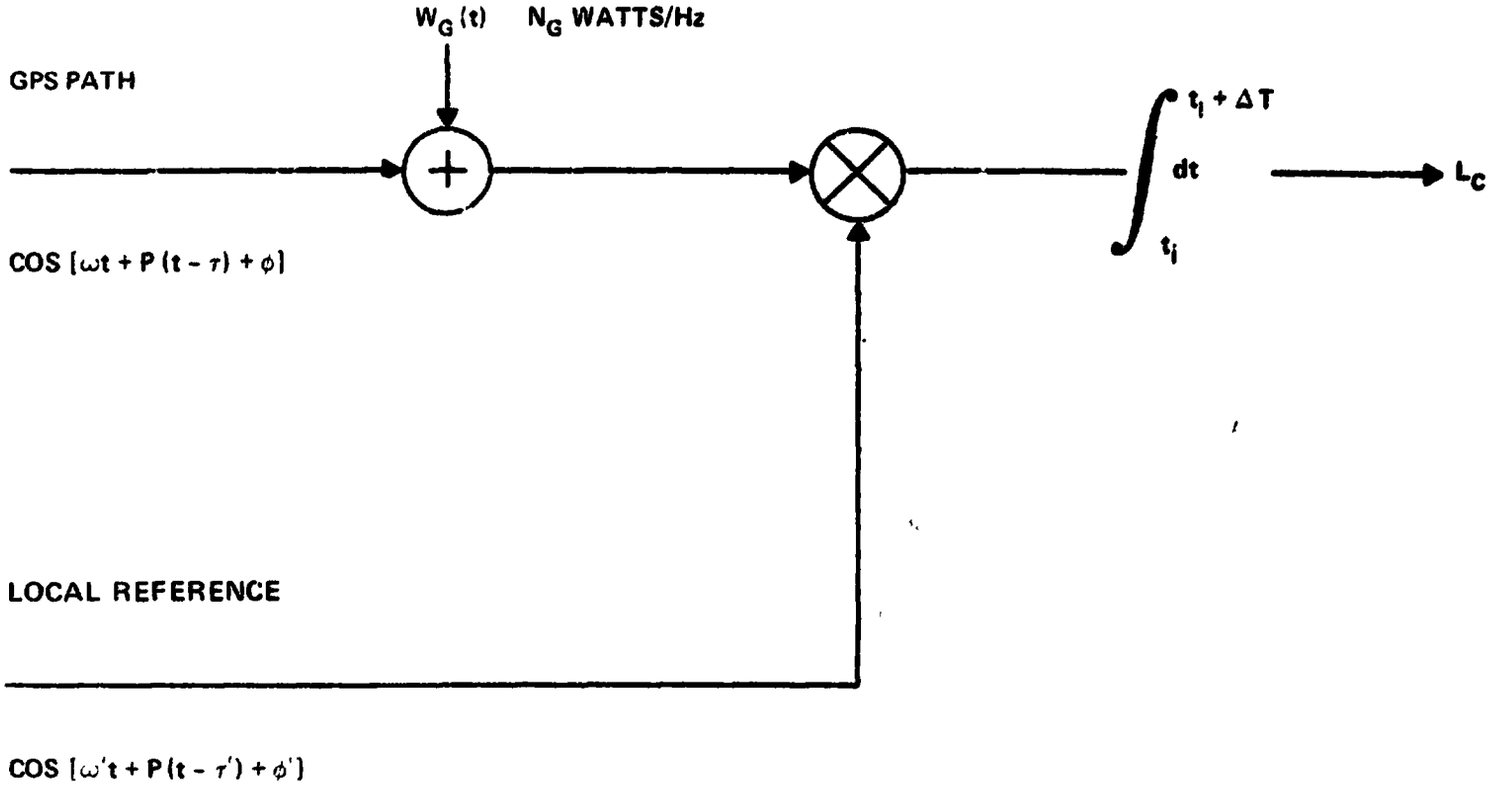

Figure 10. Equivalent Noise Model

We define function R(·), the autocorrelation of the sequence P'(·) as,

$$R(\tau - \tau') \equiv \frac{1}{N\Delta\tau}\int_{t}^{t + N\Delta\tau} P'(t - \tau)P'(t - \tau')dt, \tag{21}$$

where N is the PRN code period and $\Delta\tau$ is the duration of one "chip". The product function $P'(t - \tau)\cdot P'(t - \tau')$ contains spectral components at multiples of the basic PRN period. In the case under study these components start at DC and run to several MHz. Their spacing is approximately one kHz. The non-DC terms are classified as "self-noise." It is easy to show that the DC term is given by (21). For large processing gain (i.e., integration periods on the order of one code period or larger) we may neglect all but this term. One then has for the above expectations:

$$E[L_S|\omega_e, \tau_e] = R(\tau_e)\int_{t_i}^{t_i + \Delta T} \cos[\omega t + \phi]\cos[\omega' t + \phi']dt \tag{22}$$

$$E[L_C|\omega_e, \tau_e] = R(\tau_e)\int_{t_i}^{t_i + \Delta T} \cos[\omega t + \phi]\sin[\omega' t + \phi']dt \tag{23}$$

We express the integrands in terms of difference and double frequency terms. For $\Delta T = 10^{-3}$ sec and $\omega = 2\pi \times 10^9$ rad/sec, the double frequency term may be neglected. After integration we have:

$$E[L_S|\omega_e, \tau_e] = 1/2\ \frac{R(\tau_e)}{\omega_e}\left\{\sin[\alpha + \omega_e\Delta T] - \sin\alpha\right\} \tag{24}$$

$$E[L_C|\omega_e, \tau_e] = 1/2\ \frac{R(\tau_e)}{\omega_e}\left\{\cos[\alpha + \omega_e\Delta T] - \cos\alpha\right\} \tag{25}$$

where

$$\alpha \equiv \omega_e t_i + (\phi - \phi')$$

In a similar fashion we may compute the (equal) variances for L_S and L_C as,

$$\sigma^2 = \frac{N_G}{2}\Delta T \tag{26}$$

We can show that the two random variables are statistically independent by showing orthogonolity of the in-phase and quadrature reference signals in the interval $[t_i, t_i + \Delta T]$;

$$\int_{t_i}^{t_i + \Delta T} \cos[\omega' t + P(t - \tau') + \phi'] \sin[\omega' t + P(t - \tau') + \phi'] dt = \tag{27}$$

$$1/2 \int_{t_i}^{t_i + \Delta T} \sin[2\omega' t + 2P(t - \tau') + 2\phi'] dt \approx 0.$$

The density function for the (root) sum-square test statistic is then readily shown to be[6];

$$p_{\Lambda^{1/2}}(z) = \frac{z}{\sigma^2} \exp - [z^2 + \eta^2]/2\sigma^2 \, I_0\left(\frac{z\eta}{\sigma^2}\right) \tag{28}$$

where

$$\eta \equiv \sqrt{E[L_S|\omega_e, \tau_e]^2 + E[L_C|\omega_e, \tau_e]^2}$$

Now returning to the acquisition problem, the basic event probability of interest is:

$$P_H[E] \equiv P_r[\Lambda(i,j|\tau_e, \omega_e) > \Lambda(i^*,j|\tau_e, \omega_e)] \tag{29}$$

where i^* is the code delay step which minimizes τ_e, and i is a code delay step earlier or later than i^*. This probability can be developed using the density of Eq. (28), or by a derivation from Van Trees[7]. Using the latter we have:

$$P[x_1^2 + x_2^2 > x_3^2 + x_4^2] = 1/2[1 - Q(\beta, \alpha) + Q(\alpha, \beta)] \tag{30}$$

where Q(,) is the Marcum-Q function, x_i are Gaussian, and

$$\alpha \equiv \left[\frac{x_1^2 + x_2^2}{2\sigma^2}\right]^{1/2}$$

$$\beta \equiv \left[\frac{x_3^2 + x_4^2}{2\sigma^2}\right]^{1/2}.$$

Applying this directly to Eq. (29), we note from Eq. (24) and the sharp autocorrelation function $R(\cdot)$, that $\alpha = 0$. Further, combining Eqs. (24), (25) and (26) we have for β^2;

$$\beta^2 = \frac{R^2(\tau_e)\left\{\frac{\sin[\omega_e \Delta T]}{[\omega_e \Delta T]}\right\}^2}{\frac{N_G}{\Delta T}} \tag{31}$$

Applying standard identities for the Marcum-Q function we then have,

$$P_H[E] = 1/2\, e^{-\beta^2/2} \tag{32}$$

This function is shown in Figure 11 for a range of delay detuning values, parameterized in CNR and frequency detuning.

Lastly, we wish to discuss in more detail the interpolation function I_A of Section IV. The quantity desired is the variance of I_A, $\sigma_{I_A}^2$. For convenience we reproduced Eq. (7) below:

$$I_A = \left\{1 - \frac{[\Lambda_A(i,j)]^{1/2} - [\Lambda_A(i+1,j)]^{1/2}}{[\Lambda_A(i,j)]^{1/2} + [\Lambda_A(i+1,j)]^{1/2}}\right\}\frac{\Delta\tau}{2} \tag{33}$$

This is a function of four random variables with densities of the form of Eq. (28). The two variables in the denominator, under noiseless conditions and with unit-amplitude received carrier, sum to unity as seen in Figure 9b. For the range of CNR and integration times of interest, it is reasonable to assume that the noise contribution in the denominator is much smaller than unity. Now in the numerator, we have the difference of two (positive) random variables. For $\tau_e = \Delta\tau/2$ their expectations cancel. The variance of interest is then, approximately;

$$\sigma_{I_A}^2 \approx \left(\frac{\Delta\tau}{2}\right)^2 \cdot 2\sigma_{\Lambda^{1/2}}^2 \tag{34}$$

We can over-bound $\sigma_{\Lambda^{1/2}}^2$ with σ^2 from Eq. (26).

ACKNOWLEDGMENT

The authors appreciate the review comments by Charles E. Cote and Daniel L. Brandel of the NASA-Goddard Space Flight Center, Greenbelt, Maryland.

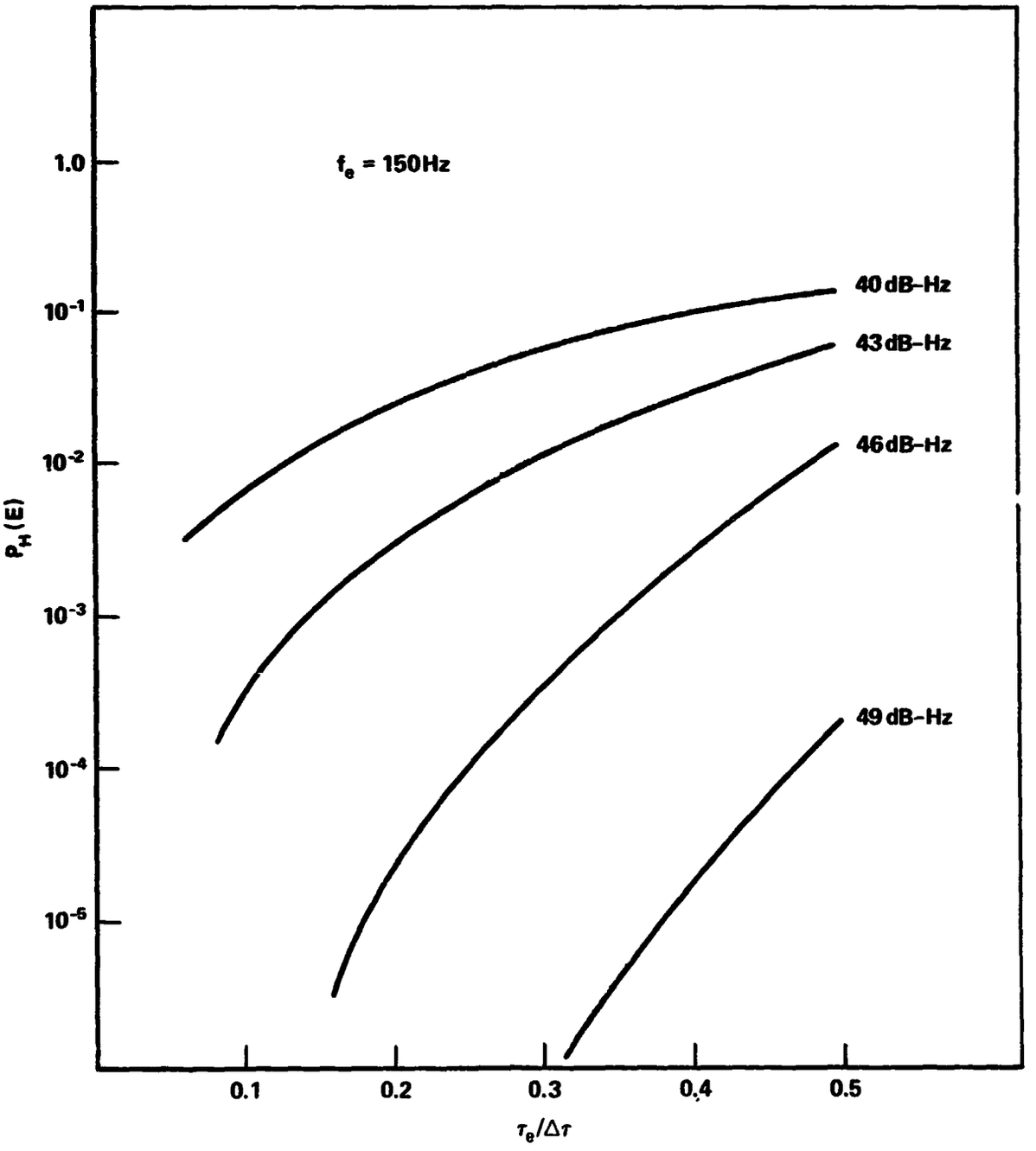

Figure 11. False Index Probability vs. Delay Error

REFERENCES

1. Milliken, R. J. and Zoller, C. J. "Principle of Operation of NAVSTAR and System Characteristics," Journal Institute of Navigation, Vol. 25, No. 2, Summer 1978, pp. 95–106.

2. Spilker, J. J., "Signal Structure and Performance Characteristics," Journal Institute of Navigation, Vol. 25, No. 2, Summer 1978, pp. 121–146.

3. Glazer, B. G., "GPS Receiver Operation," Journal Institute of Navigation, Vol. 25, No. 2, Summer 1978, pp. 173–178.

4. Stansell, T. A., "Civil Marine Applications of the Global Positioning System," Journal Institute of Navigation, Vol. 25, No. 2, Summer 1978, pp. 224–235.

5. Spilker, J. J., "Delay-lock tracking of binary signals," IRE Trans. on Space Electronics and Telemetry, Vol. SET-9, pp. 1–3, March 1963.

6. Probability, Random Variables and Stochastic Processes, Papoulis, McGraw-Hill, pp. 195–196.

7. Detection, Estimation, and Modulation Theory, Part I, Van Trees, H. L., pp. 394–395, Wiley, New York, 1968.

Table 3
Summary of Notation

$\Lambda_A(i,j)$	Test statistic for GPS satellite A generated with delay step i and VXCO step j.
$\hat{\underline{i}} = [\hat{i}_A, \hat{i}_B, \hat{i}_C, \hat{i}_D]$	Maximum-likelihood code delay steps for GPS satellites A, B, C, and D.
τ_e	Code Delay Off-set Error.
$\Delta\tau$	Delay time step size.
I_A, I_B, I_C, I_D	Delay interpolation constants.
$\hat{\underline{j}} = [\hat{j}_A, \hat{j}_B, \hat{j}_C, \hat{j}_D]$	Maximum-likelihood frequency steps for GPS satellites A, B, C, and D.
$\Delta\omega$	VCXO angular frequency step size.
ω_{GPS}	Carrier frequency emitted at GPS satellite.
ω_{RS}	Carrier frequency emitted at REFSAT.
ω_{LO}	Receiver LO frequency.
ω_e	Frequency de-tuning error.
T_{RS}	Start time of REFSAT frame sync word at REFSAT satellite.
ΔT	Statistic integration time.
$\underline{r}_A$	Positions of GPS satellite A.
$\dot{\underline{r}}_A$	GPS satellite A velocity.
$\hat{\underline{r}}_o$	User Terminal position estimate.
$\hat{\underline{r}}_o$	User Terminal velocity estimate.
P(t)	C/A code waveform.
$w_G(t)$	Noise waveform at GPS Channel IF output, unity amplitude signal reference.
N_G	Noise spectral density at GPS Channel IF output.
L_C, L_S	In-phase (cosine) and quadrature (sine) integrator outputs.
ϕ	Phase error.
σ^2	Variance of integrator outputs.
N	Number of chips in C/A code.

Table 3 (Continued)

$R(\ )$	Autocorrelation of C/A code.
α, β	Error exponents.
$P_H[E]$	False index error probability.
$Q(\ ,\ )$	Marcum-Q function.
σ_I^2	Delay interpolation error variance.
C	Propagation velocity.